Topology-Aware Quality Control of Triangulated Terrain Models Using Local Euler Curvature and Elevation-Filtration Curves

Bekarys Tashmukhanbet Bazarbekuly
Nazarbayev Intellectual School of Physics and Mathematics, Almaty, Kazakhstan
bekovbekarys@gmail.com

Corresponding author: Bekarys Tashmukhanbet Bazarbekuly, bekovbekarys@gmail.com

Peer review status

This is a non-peer-reviewed preprint submitted to EarthArXiv.

This manuscript has been submitted for publication in International Journal of Geosciences.

Topology-Aware Quality Control of Triangulated Terrain Models Using Local Euler Curvature and Elevation-Filtration Curves

Bekarys Tashmukhanbet Bazarbekuly

Nazarbayev Intellectual School of Physics and Mathematics, Almaty, Kazakhstan
Email: bekovbekarys@gmail.com

Abstract

Triangulated irregular networks (TINs) are widely used to represent topography and bathymetry, but their quality control is usually dominated by geometric criteria such as minimum angle and aspect ratio, which do not test whether connectivity errors have changed the topology of the mesh. We present a topology-aware quality-control framework based on a local Euler-curvature identity and on lower-star Euler characteristic curves (ECCs). For a triangular two-manifold with boundary we classify the affine local functionals of vertex degree, incident-face count and boundary indicator whose total is invariant under mesh refinement and boundary discretization, and reduce them to the canonical normalization $\kappa_\chi(v) = 1 - d(v)/2 + t(v)/3$, whose sum equals the Euler characteristic of any finite triangular complex. Across 32 valid meshes built from four triangulation rules and four resolutions on two real Earth-surface benchmark arrays, the largest static residual was 1.74×10^{-11}. Injecting 1 to 40 missing facets, duplicated facets or orphan vertices returned a residual equal to the number of defects, whereas topology-preserving diagonal remeshing left it at machine precision. A coordinate-only sliver collapsed the minimum plan-view angle from 38.75° to 0.28° without changing the topological residual. ECCs additionally exposed representation uncertainty, with maximum inter-triangulation spreads of 25 and 20 Euler units and raster 4- versus 8-neighbour differences of 80 and 70. The framework separates mesh topology, element geometry and representation-induced uncertainty in an auditable way.

Keywords

Triangulated Irregular Network, Digital Elevation Model, Euler Characteristic, Mesh Quality, Topological Data Analysis

1. Introduction

Triangular meshes are a basic representation of Earth surfaces. They appear in terrain generalization and geomorphometry, variable-resolution land-surface and hydrological models, and unstructured coastal-ocean models [1] [2]. Compared with a fixed raster, a triangulated irregular network (TIN) can allocate vertices according to terrain complexity and can encode breaklines and boundaries explicitly. This flexibility, however, also makes connectivity part of the data model. Two meshes can use the same sampled elevations while assigning different diagonals, boundaries or local connectivity, and downstream analysis may therefore depend on choices made during mesh construction.

Most mesh-quality pipelines emphasize geometry: triangle angles, aspect ratios, skewness, interpolation error or feature-preservation criteria. These quantities are indispensable, but they answer a different question from whether the discrete complex has the intended topology. A mesh may have well-shaped triangles yet contain a missing facet or an unintended hole. Conversely, a mesh can retain exactly the intended topology while containing a near-degenerate sliver. Earth-science workflows would benefit from a lightweight, auditable topology check that is mathematically exact and computationally inexpensive.

Discrete differential geometry provides a natural starting point. Smooth Gauss–Bonnet relates integrated Gaussian and boundary curvature to the Euler characteristic [3]; discrete analogues distribute curvature over vertices of polyhedral surfaces and planar graphs [4]-[7]. In terrain analysis, triangle-mesh curvature has been used to approximate metric Gaussian and mean curvature and to identify geomorphic features [8] [9]. The purpose of the present work is deliberately different: rather than estimating physical surface bending from triangle angles or heights, we use a combinatorial curvature as an accounting device for mesh topology.

A second motivation comes from topological data analysis (TDA). Persistent homology and related methods have been used with terrain and LiDAR data, including landslide detection [10]. Euler characteristic curves (ECCs) provide a cheaper topological summary of a scalar filtration and can be computed efficiently even for large data sets [11]. For a terrain TIN, filtering simplices by elevation produces an ECC that records how the topology of the sublevel terrain changes from low to high elevations. Unlike the final Euler characteristic, the intermediate curve is sensitive to how sampled points are connected, making it useful for quantifying representation uncertainty.

This study develops a combined static and filtration-based framework. The contributions are fourfold.

1) We derive the complete boundary-aware affine family of local degree/face-count functionals whose total is invariant under triangular-mesh refinement, and reduce it to a canonical local Euler curvature.

2) We turn the identity into a static topology audit R_χ and demonstrate its complementary role alongside geometric triangle quality.

3) We define an elevation lower-star ECC protocol for TINs and use multiple valid triangulations to quantify connectivity-induced uncertainty.

4) We provide a fully reproducible Python implementation and evaluate it on two real Earth-surface benchmark arrays, multiple resolutions and controlled mesh-corruption experiments.

The intended contribution is therefore methodological and informatic rather than a claim that combinatorial curvature is a new estimator of geomorphic curvature. The numerical experiments are designed to test invariance, failure modes and representation sensitivity, not to infer new geology from the two benchmark regions.

2. Mathematical Framework

2.1. Triangular Terrain Complex and Notation

Let $K = (\mathscr{F}, \mathscr{E}, \mathbb{R})$ be a finite triangular two-dimensional complex representing a terrain patch, and let V, E and F denote the numbers of its vertices, unique edges and triangular faces. The Euler characteristic of the complex is $\chi(K) = V - E + F$. For a vertex v, write $d(v)$ for the number of incident unique edges and $t(v)$ for the number of incident triangular faces. If K is a two-manifold with boundary, let $b(v) = 1$ for boundary vertices and $b(v) = 0$ otherwise, and let L denote the number of boundary edges. Each polygonal boundary component has equally many vertices and edges, so the boundary indicators sum to L. Consider the affine local functional given in Equation (1).

$$\kappa(v) = A + B\,d(v) + \frac{C}{3}\,t(v) + T\,b(v) \tag{1}$$

The normalization by 1/3 is convenient because each triangular face is counted at exactly three vertices.

2.2. Classification of Refinement-Invariant Affine Functionals

For a triangular two-manifold with boundary, the incidence sums are given by Equation (2).

$$\sum_v d(v)=2E, \sum_v t(v)=3F, \sum_v b(v)=L \tag{2}$$

Therefore the total of the local functional is given by Equation (3).

$$\sum_v \kappa(v)=AV+2BE+CF+TL \tag{3}$$

The incidence and Euler relations are given by Equation (4).

$$3F=2E-L, V-E+F=\chi \tag{4}$$

Solving Equation (4) for E and F gives Equation (5).

$$E=3V-L-3\chi, F=2V-L-2\chi \tag{5}$$

Substitution into Equation (3) yields Equation (6).

$$\sum_v \kappa(v)=(A+6B+2C)V+(T-2B-C)L-(6B+2C)\chi \tag{6}$$

Theorem 1 (Boundary-aware affine classification). For the class of finite triangular two-manifolds with boundary of fixed topology, the total of Equation (1) is independent of interior refinement and boundary subdivision if and only if the conditions of Equation (7) hold.

$$A+6B+2C=0, T=2B+C \tag{7}$$

Under these conditions the total is given by Equation (8).

$$\sum_v \kappa(v)=-(6B+2C)\chi(K) \tag{8}$$

Proof. Sufficiency follows directly from Equation (6). For necessity, perform two topology-preserving local operations. First, stellar subdivision of an interior triangle adds one vertex, three edges and two faces while leaving L and χ unchanged. Invariance therefore requires $A + 6B + 2C = 0$. Second, split a boundary edge and its incident triangle by inserting a vertex on that edge. This changes (V, E, F, L) by $(1, 2, 1, 1)$ without changing χ. Hence $A + 4B + C + T = 0$; combining this with the first condition gives $T = 2B + C$.

The result can be interpreted as a boundary-aware affine form of Euler accounting. On a genuine triangular two-manifold, the apparent two-parameter family collapses locally to a single scale. Put $u = B + C/3$. At an interior vertex $t(v) = d(v)$; at a boundary vertex $t(v) = d(v) - 1$. Using Equation (7), the functional reduces to Equation (9).

$$\kappa(v)=\begin{cases} u[d(v)-6], & v\notin\partial K \\ u[d(v)-4], & v\in\partial K \end{cases} \tag{9}$$

Choosing $u = -1/6$ gives the canonical normalized form of Equation (10).

$$\kappa_\chi(v)=1-\frac{d(v)}{2}+\frac{t(v)}{3} \tag{10}$$

For a manifold, this is $(6 - d)/6$ in the interior and $(4 - d)/6$ on the boundary.

Corollary 1 (Local Euler accounting). For any finite triangular complex, even when it is not a two-manifold, the functional in Equation (10) satisfies Equation (11).

$$\sum_{v \in V} \kappa_\chi(v) = V - E + F = \chi(K) \tag{11}$$

Proof. Summing the three terms in Equation (10) gives V − (1/2) times the total vertex degree plus (1/3) times the total face incidence, which equals $V - E + F$, because every edge has two endpoints and every triangular face has three vertices.

This corollary is especially useful for quality control because the local contributions can be recomputed directly from the mesh data structure and checked against an independently specified expected topology.

2.3. What the Local Curvature Is, and Is Not

The quantity $\kappa_\chi(v)$ depends only on connectivity. It does not use x, y, z, triangle angles or edge lengths. It must therefore not be interpreted as Gaussian, mean, profile or plan curvature of the physical terrain. Metric discrete curvature methods use angle defects or other geometric operators [7] [8] [9]. Here the robust invariant is the sum in Equation (11); the local allocation can move between vertices when diagonals are changed. We quantify this local sensitivity explicitly in Section 4.2.

3. Materials and Methods

3.1. Earth-Surface Benchmark Data

Two real-world gridded elevation examples were used (**Figure 1**). Both are distributed as sample data with Matplotlib and are included verbatim in the supplementary reproducibility package used for this study [12]. They are used as computational benchmarks, not as authoritative survey products for new geological interpretation.

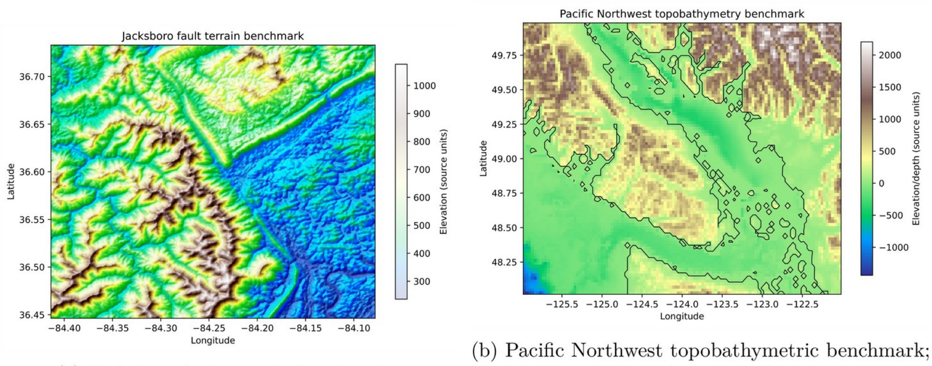

(a) Jacksboro-fault terrain benchmark.

(b) Pacific Northwest topobathymetric benchmark; the black contour marks zero in the source array.

Figure 1. Real Earth-surface benchmark arrays used in the experiments: (a) Jacksboro-fault terrain benchmark; (b) Pacific Northwest topobathymetric benchmark, in which the black contour marks zero in the source array. The panels are visualizations of the supplied numerical arrays; no generative imagery was used.

The first data set, jacksboro_fault_dem.npz, contains a 344 × 403 terrain array (138,632 samples) spanning longitude −84.41375° to −84.07792° and latitude 36.44625° to 36.73292°. Array values range from 236 to 1076 in the source data units. The region lies in the Appalachian Jacksboro-fault area, whose structural geology is described by U.S. Geological Survey mapping and synthesis [13]. The second data set, topobathy.npz, contains a 91 × 120 topobathymetric array (10,920 samples) spanning approximately −125.9833° to −122.0166° and 48.0164° to 49.9842° in the Pacific Northwest. Values range from −1437 to 2205 in the source units. Because the bundled sample files do not carry full survey-level provenance or vertical-datum metadata, we report vertical values as source units and do not make process-level geomorphic claims from their magnitudes.

3.2. TIN Construction and Resolution Ensemble

Each rectangular cell was divided into two triangles. Four connectivity rules were tested while retaining exactly the same grid vertices and elevations:

- **Main diagonal**: top-left to bottom-right in every cell;
- **Anti-diagonal**: top-right to bottom-left in every cell;
- **Checkerboard**: alternating main and anti diagonals by row and column parity;
- **Adaptive**: the diagonal whose two endpoints have the smaller absolute elevation difference.

The first three isolate pure connectivity choices, whereas the adaptive rule is a simple terrain-dependent heuristic. It is not proposed as an optimal TIN algorithm; it is used to create a fourth valid representation against which topological sensitivity can be measured.

Resolution sensitivity was tested by regularly subsampling each raster with strides 1, 2, 4 and 8 before triangulation. This generated 16 valid meshes per benchmark and 32 valid meshes in total. Plan coordinates for geometric quality calculations were converted from longitude/latitude to local equirectangular coordinates using the mean latitude of each benchmark extent. Over these compact extents this is sufficient for triangle-shape diagnostics; elevation was not included in the plan-view shape-quality calculation.

3.3. Static Topology Audit

For an intended simply connected terrain patch with one outer boundary and no holes, the expected Euler characteristic is $\chi_{expected} = 1$. We define the static residual as in Equation (12).

$$R_\chi = \left| \sum_v \kappa_\chi(v) - \chi_{\text{expected}} \right| \tag{12}$$

A valid disk-like mesh should have $R_\chi = 0$ up to floating-point roundoff. For a legitimate domain with h holes and one connected component, the expected value must instead be $1 - h$; for multiple components or more general complexes, the expected topology must be supplied appropriately. Thus R_χ is not a universal “bad mesh” score: it is a consistency test between the encoded complex and the topology intended by the modeler.

3.4. Geometric Quality Companion

Topology alone cannot identify poor triangle shapes. For each plan-view triangle with side lengths a, b, c and area $A_\triangle$, we computed the minimum internal angle and the shape measure of Equation (13).

$$q = \frac{4\sqrt{3}\,A_\triangle}{a^2 + b^2 + c^2} \tag{13}$$

Here $q = 1$ for an equilateral triangle and approaches zero for a degenerate triangle. The topological residual and geometric measures are intentionally kept as separate channels.

3.5. Elevation-Filtration Euler Characteristic Curves

Static χ tests the topology of the complete complex but contains no information about how terrain connectivity changes with elevation. To retain this information, we use the lower-star filtration induced by vertex elevation z. At threshold h, the sublevel complex is defined by Equation (14).

$$K_h = \left\{ \sigma \in K : \max_{v \in \sigma} z(v) \le h \right\} \tag{14}$$

The Euler characteristic curve is then given by Equation (15).

$$ECC(h)=\chi(K_h)=V_h-E_h+F_h \tag{15}$$

Computationally, a vertex is born at its elevation, an edge at the maximum elevation of its two endpoints and a triangle at the maximum elevation of its three vertices. Sorting these birth values permits exact evaluation of Equation (15) at arbitrary thresholds using cumulative counts, without persistent-homology matrix reduction. This follows the broader use of ECCs as efficient topological summaries [11] [14].

For a fixed set of vertices and elevations, the four triangulation rules produce a representation ensemble. At each threshold we define the triangulation-uncertainty envelope of Equation (16).

$$U(h)=\max_r \chi\left(K_h^{(r)}\right)-\min_r \chi\left(K_h^{(r)}\right) \tag{16}$$

We report its mean and maximum, as well as pairwise mean absolute ECC differences. Because all four full complexes are topological disks, all curves terminate at $\chi = 1$; disagreement at intermediate thresholds reflects connectivity choices, especially near discrete saddle configurations.

3.6. Resolution Sensitivity

For the adaptive triangulation, ECCs were recomputed for strides 1, 2, 4 and 8 on a common set of 401 thresholds spanning the full elevation range. Since vertex count changes substantially with resolution, we compared normalized curves $\chi(K_{*h*})/V$. Relative to the stride-1 curve, we report root-mean-square error (RMSE) and mean absolute error (MAE), multiplied by 10^4 for readable values.

3.7. Controlled Corruption and Negative Controls

Controlled defects were injected into the stride-4 Jacksboro mesh. Isolated interior triangles sharing no vertices were selected with a fixed random seed. For k = 1, 2, 5, 10, 20 and 40 we tested three topological corruption families:

1) delete k isolated interior faces;
2) duplicate k faces while retaining the same unique edge set;
3) add k explicit orphan vertices with no incident simplex.

These are intentionally simple unit tests of accounting failure modes, not a statistical model of all errors found in production GIS files. Two negative and complementary controls were also used. First, all cell diagonals were reversed, changing local connectivity while preserving global topology. Second, one interior plan-view vertex was moved to 1% of its original distance from its eastern neighbour, creating a severe sliver without changing connectivity. This separates the expected responses of topological and geometric quality checks.

For the 10-missing-face case, the local difference of Equation (17) was also mapped to determine whether a known-good reference mesh permits localization of the affected one-rings.

$$\Delta\kappa_\chi(v)=\kappa_\chi^{\text{corrupt}}(v)-\kappa_\chi^{\text{baseline}}(v) \tag{17}$$

3.8. Raster-Connectivity Comparison

Binary raster topology itself depends on a connectivity convention. As a contextual comparison, for each elevation threshold we binarized the raster sublevel set and evaluated its Euler characteristic with 4-neighbour and 8-neighbour foreground connectivity using scikit-image [15]. We compared the resulting raster curves with the adaptive TIN ECC. This experiment is not a claim that one connectivity is universally correct; it quantifies the magnitude of the representation choice on the same scalar field.

3.9. Implementation and Reproducibility

All calculations were performed in Python using NumPy for array operations [16], Matplotlib for visualization

[12] and scikit-image for the raster-connectivity comparison [15]. The core mesh code constructs triangles, extracts unique edges, counts incidences, evaluates Equation (10), computes triangle quality and evaluates ECCs. Exact input arrays, scripts, generated CSV/JSON tables and publication figures are supplied with the submission package. No numerical result in this paper was manually entered before computation; manuscript values were taken from the generated result files.

4. Results

4.1. Static Invariance on Valid Earth-Surface Meshes

All 32 valid TINs had $\chi = 1$ and a local curvature total of 1 to numerical precision. The maximum absolute residual across all triangulation rules and resolutions was 1.74×10^{-11} for Jacksboro and 1.33×10^{-12} for the topobathy benchmark. Full-resolution mesh statistics are summarized in **Table 1**.

Table 1. Full-resolution static mesh statistics for the main-diagonal triangulation. The final column reports the maximum R_χ observed over all four triangulation rules and all four tested strides for that data set.

Data set	V	E	F	Boundary edges	Min angle (deg)	q_{min}	Max R_χ
Jacksboro	138,632	414,403	275,772	1490	38.75	0.8455	1.74×10^{-11}
Topobathy	10,920	32,339	21,420	418	44.37	0.8658	1.33×10^{-12}

The invariance is expected from Equation (11), but the real-data experiment verifies that the implementation respects it across substantially different vertex counts and connectivity rules. It also provides a baseline against which deliberately corrupted inputs can be evaluated.

4.2. Local Curvature Is Connectivity-Sensitive

Although the total is invariant, local $\kappa_\chi(v)$ values are not. On the Jacksboro stride-2 mesh, 38.97% of vertices changed κ_χ between the main and adaptive triangulations, with RMSE 0.1229 and maximum absolute change 1/3. Between checkerboard and adaptive triangulations, 97.12% changed, with RMSE 0.3535 and maximum change 2/3. On the full-resolution topobathy mesh, the corresponding changed fractions were 48.86% and 95.66%, with RMSE 0.1433 and 0.3633. These results reinforce the interpretation in Section 2.3: local combinatorial Euler curvature is an incidence allocation, not a triangulation-independent terrain-shape observable.

4.3. Triangulation Uncertainty in Elevation Filtrations

The ECCs agreed at the final threshold but differed substantially at intermediate elevations (**Figure 2** and **Figure 3**). For Jacksboro at stride 2 (V = 34,744), the mean uncertainty-envelope width was 6.44 Euler units and the maximum was 25 at source elevation 351.99. The maximum is 7.20 Euler units per 10,000 vertices. Pairwise ECC mean absolute differences ranged from 2.77 (main versus checkerboard) to 4.71 (main versus anti-diagonal).

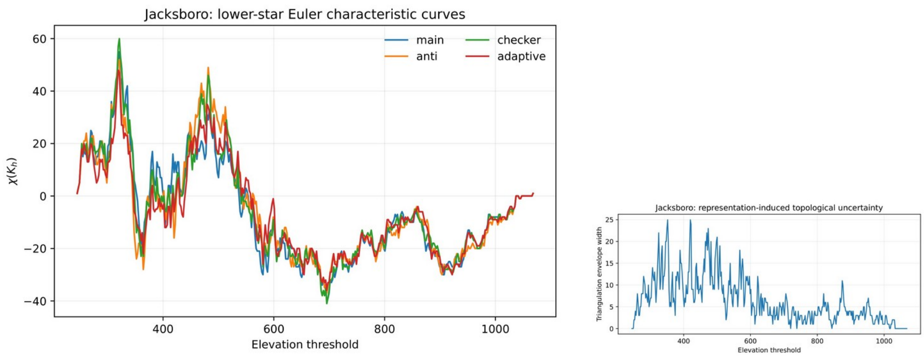

(a) ECCs under four valid triangulations. (b) Envelope width $U(h)$.

Figure 2. Jacksboro-fault benchmark at stride 2: (a) ECCs under four valid triangulations; (b) envelope width $U(h)$. All representations end at $\chi = 1$, while intermediate sublevel topology depends on diagonal assignment.

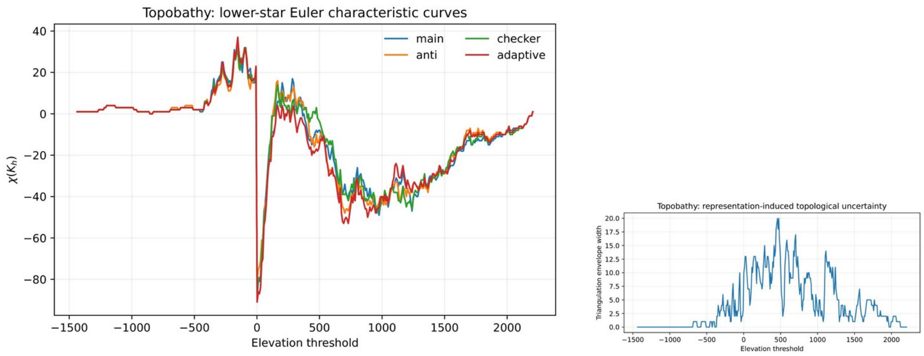

(a) ECCs under four valid triangulations. (b) Envelope width $U(h)$.

Figure 3. Pacific Northwest topobathymetric benchmark at full resolution: (a) ECCs under four valid triangulations; (b) envelope width $U(h)$. Connectivity uncertainty is zero at the complete-complex endpoint but nonzero over many elevation thresholds.

For the full-resolution topobathy surface (V = 10,920), mean envelope width was 4.27 and maximum width was 20 at source value 456.84, or 18.32 per 10,000 vertices. Pairwise mean absolute differences ranged from 2.01 (main versus checkerboard) to 3.03 (checkerboard versus adaptive). These differences arise despite identical sampled elevations and identical final topology. Selected connectivity-sensitivity statistics for both benchmarks are collected in **Table 2**.

Table 2. Selected connectivity-sensitivity statistics. "Changed" is the fraction of vertices whose local κ_χ differs between the named triangulations. ECC envelope values are evaluated across all four triangulations.

Data set	Comparison	Changed (%)	Local RMSE	Mean U	Max U
Jacksboro (stride 2)	main–adaptive	38.97	0.1229	6.44	25
Jacksboro (stride 2)	checker–adaptive	97.12	0.3535	6.44	25
Topobathy (stride 1)	main–adaptive	48.86	0.1433	4.27	20
Topobathy (stride 1)	checker–adaptive	95.66	0.3633	4.27	20

4.4. Resolution Sensitivity of Normalized ECCs

Coarsening changed the normalized ECC increasingly strongly (**Figure 4**; **Table 3**). For Jacksboro, RMSE relative to the full-resolution normalized curve increased from 3.94 per 10,000 vertices at stride 2 to 58.40 at stride 8. The topobathymetric surface increased from 13.78 to 107.07 over the same stride sequence. The effect is therefore data dependent and cannot be removed by normalizing only by vertex count.

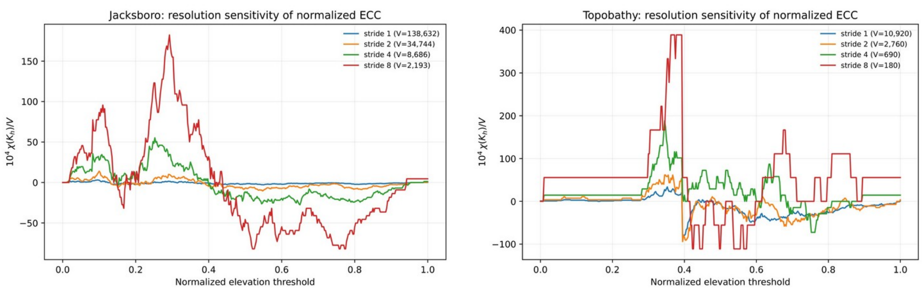

(a) Jacksboro. (b) Topobathy.

Figure 4. Resolution sensitivity of adaptive-triangulation ECCs, normalized by vertex count, for (a) Jacksboro and (b) topobathy. Thresholds are normalized to each benchmark's vertical range for display.

Table 3. Resolution sensitivity of the adaptive-triangulation normalized ECC. RMSE and MAE are relative to stride 1 and are multiplied by 10^4.

Data set	Stride	Vertices	RMSE	MAE
Jacksboro	1	138,632	0.00	0.00
	2	34,744	3.94	3.31
	4	8686	18.76	15.77
	8	2193	58.40	46.95
Topobathy	1	10,920	0.00	0.00
	2	2760	13.78	9.42
	4	690	46.31	34.69
	8	180	107.07	80.68

4.5. Controlled Topology Corruption

The static audit responded linearly to all three injected topological error families (**Figure 5**). Deleting k isolated interior triangles changed χ from 1 to $1 - k$; duplicating k faces or adding k orphan vertices changed it from 1 to $1 + k$. In each case $R_\chi = k$ up to floating-point roundoff for k = 1, 2, 5, 10, 20 and 40. For example, with 10 defects, missing faces gave $\chi = -9$ and a curvature total of −9, while duplicates and orphan vertices each gave $\chi = 11$ and a curvature total of 11. Because R_χ was evaluated against the intended disk topology, all three produced a residual of 10.

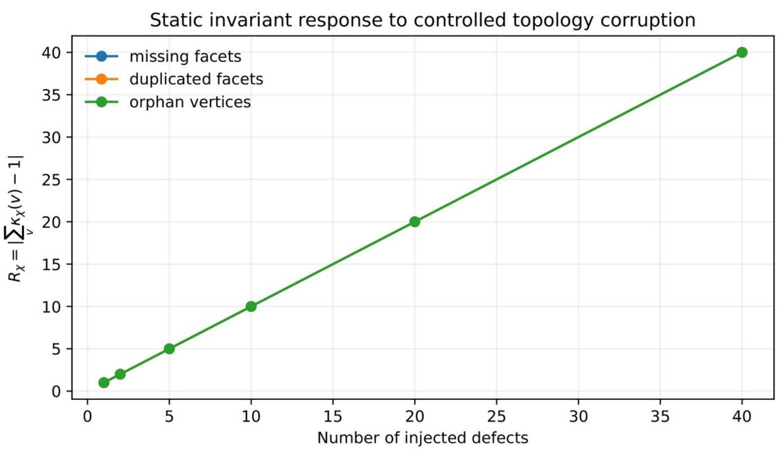

Figure 5. Response of the static topology residual to controlled corruption of the stride-4 Jacksboro mesh. The identity line arises from the exact change in $V - E + F$ for the injected unit defects.

By contrast, reversing all 8500 cell diagonals of the stride-4 mesh retained $\chi = 1$ and $R_\chi = 1.11 \times 10^{-16}$. This is an important negative control: the static audit is intentionally invariant to topology-preserving remeshing and therefore should not be presented as a detector of every connectivity change.

4.6. Topological and Geometric Quality Assurance Are Complementary

The coordinate-sliver control preserved the exact connectivity of the baseline mesh, leaving $\chi = 1$ and $R_\chi = 1.11 \times 10^{-16}$. However, its minimum plan-view angle fell from 38.7495° to 0.2808°, and q_{min} fell from 0.84549 to 0.00849. Conversely, deleting 10 isolated faces changed R_χ from approximately zero to 10 while leaving the minimum angle and q_{min} of retained triangles unchanged (**Figure 6**; **Table 4**). Neither diagnostic subsumes the other.

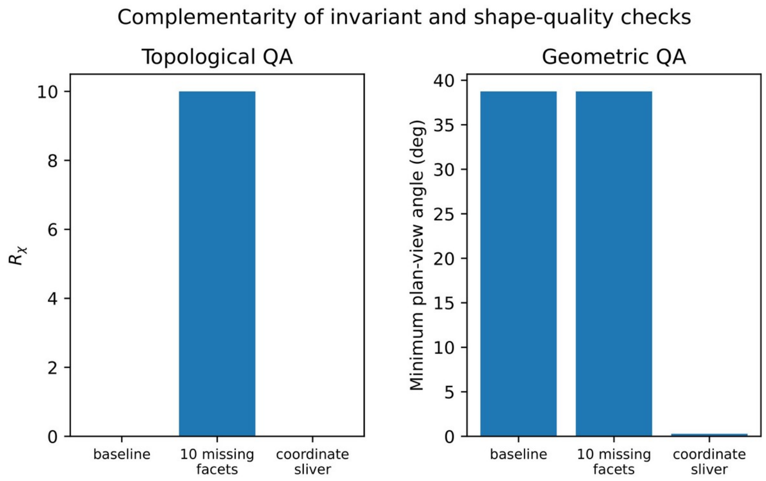

Figure 6. Complementary failure modes of topological and geometric quality checks. The missing-facet defect is detected by R_χ but not by triangle shape; the coordinate sliver is detected by minimum angle but not by R_χ.

Table 4. Selected controlled-quality cases on the stride-4 Jacksboro mesh.

Case	χ	R_χ	Min angle (deg)	q_{min}
Baseline	1	1.11×10^{-16}	38.7495	0.84549
10 missing facets	−9	10.0	38.7495	0.84549
10 duplicated facets	11	10.0	38.7495	0.84549
10 orphan vertices	11	10.0	38.7495	0.84549
8500 diagonal flips	1	1.11×10^{-16}	38.7495	0.84549
Coordinate sliver	1	1.11×10^{-16}	0.2808	0.00849

4.7. Localization with a Reference Mesh

For 10 vertex-disjoint missing interior faces, exactly 30 vertices changed local curvature relative to the baseline and every affected vertex had $\Delta\kappa_\chi = -1/3$. The changes therefore summed to −10, matching the global topological deficit. **Figure 7** shows that, when a reference connectivity is available, the local accounting difference can identify the one-rings directly affected by a missing-facet event. This localization should not be confused with terrain-feature detection: it compares two mesh data structures, not physical landform geometry.

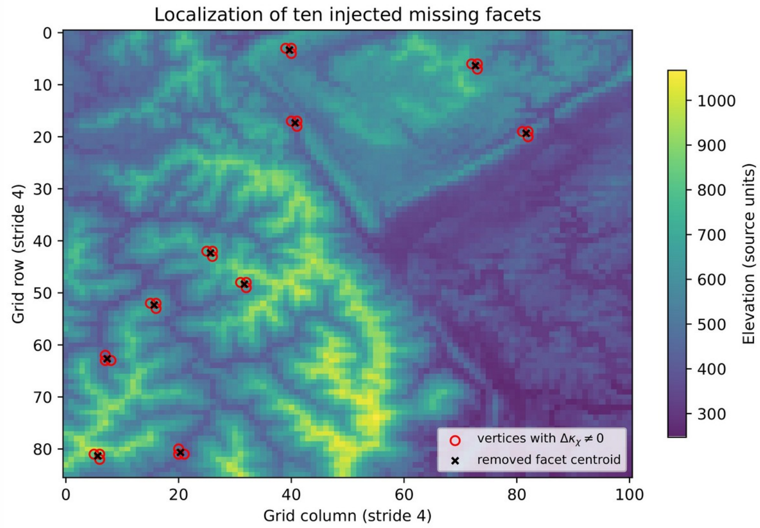

Figure 7. Local Euler-curvature difference for 10 isolated removed triangles in the Jacksboro stride-4 mesh. Thirty incident vertices change by −1/3 each, exactly accounting for the global change of −10.

4.8. Raster Connectivity Can Dominate Filtration Differences

The raster comparison confirms that topology derived from gridded elevation data also depends strongly on connectivity convention (**Figure 8**). On Jacksboro stride 2, the mean absolute difference between the 4-neighbour and 8-neighbour raster ECCs was 26.84 Euler units and the maximum difference was 80. The adaptive TIN curve had mean absolute differences of 14.02 from the 4-neighbour raster curve and 12.82 from the 8-neighbour curve. For the full-resolution topobathymetric surface, the raster 4-versus-8 mean absolute difference was 19.80 with maximum 70; the adaptive TIN differences were 11.12 and 8.67, respectively. The result demonstrates that connectivity uncertainty is not a peculiarity of TINs. It is a general discretization issue that should be made explicit when topology-derived terrain summaries are reported.

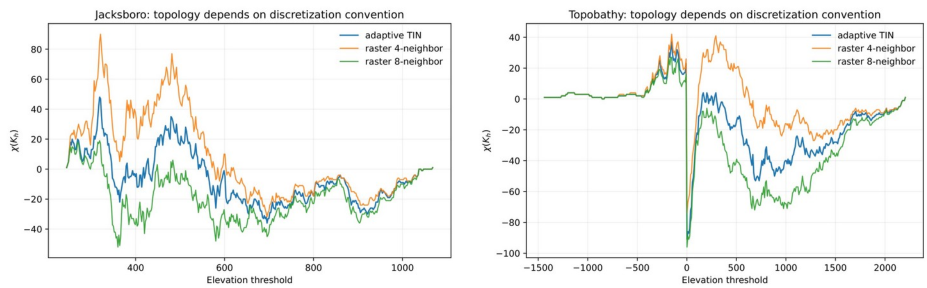

(a) Jacksboro, stride 2.

(b) Topobathy, full resolution.

Figure 8. Euler characteristic curves under adaptive TIN connectivity and two conventional raster foreground-connectivity rules for (a) Jacksboro at stride 2 and (b) topobathy at full resolution.

5. Discussion

5.1. A Practical Three-Layer Audit for Earth-Science Meshes

The experiments suggest a simple quality-control hierarchy for TIN-based Earth-science workflows.

Layer 1: static topology. Compute V, E, F, χ, the local vector $\kappa_\chi(v)$ and R_χ against the topology expected from the domain definition. This step is exact, fast and auditable. It can detect a change in Euler characteristic caused by missing components, holes, orphan vertices or analogous accounting errors, but it cannot determine whether a changed topology is intentional.

Layer 2: element geometry. Compute conventional shape-quality metrics such as minimum angle and Equation (13). The sliver experiment shows why this layer is essential: topological correctness does not imply numerical or interpolation quality. This is consistent with unstructured Earth-system modeling practice, in which mesh quality and feature-based refinement are central design objectives [1] [2].

Layer 3: filtration and representation sensitivity. When a terrain-derived topological descriptor is used scientifically, compute it across plausible representations rather than assuming a single diagonal convention is neutral. The envelope $U(h)$ is a direct way to report this uncertainty for ECCs. For regular-grid source data, raster 4/8-connectivity and TIN diagonal choices represent closely related ambiguity: they resolve local adjacency differently around thresholded cells.

The three layers answer different questions. A production pipeline should not collapse them into one score without a use-case-specific weighting scheme.

5.2. Relation to Discrete Curvature in Geomorphometry

There is an important conceptual distinction between the present method and existing terrain-curvature work. Discrete Gauss–Bonnet can be used geometrically through angle defects to approximate Gaussian curvature on a triangulated surface, and such methods can be useful for recognizing point-like terrain features [9]. Other TIN-based methods estimate gravity-specific land-surface curvatures from geometric vectors [8]. Those are metric quantities: changing vertex positions while holding connectivity fixed changes the result.

The canonical κ_χ used here is combinatorial. It is valuable precisely because it ignores metric geometry and provides an exact Euler accounting identity. Our local-sensitivity experiment further shows that its per-vertex values should not be mapped and interpreted as if they were physically meaningful curvature magnitudes independent of triangulation. A future hybrid method could report metric curvature together with local topological bookkeeping, but the two should remain named and validated separately.

5.3. ECCs as a Compact Terrain-Topology Diagnostic

ECCs sit between a single global invariant and the richer but more expensive information in persistent homology. They record the alternating simplex count over the entire elevation filtration and can be computed by sorting simplex birth values. Their weakness is also clear: different topologies can share the same Euler characteristic at a given threshold because $\chi = \beta_0 - \beta_1$ in a two-dimensional sublevel complex. Thus an ECC cannot distinguish, for example, one additional component from one additional loop if their contributions cancel. Persistent homology is preferable when the identity and lifetime of individual features matter [10] [14]. ECCs are attractive for quality control and ensemble screening because of their low computational and storage costs [11].

The present experiments also demonstrate two sources of uncertainty that should accompany any quantitative interpretation of terrain ECCs: triangulation choice and sampling resolution. The normalized ECC did not converge trivially under coarse subsampling, and the topobathy benchmark was especially sensitive. Consequently, comparing ECCs between study areas is meaningful only when resolution and construction rules are controlled or explicitly modeled.

5.4. What the Corruption Experiment Proves and What It Does Not

The linear response $R_\chi = k$ for the chosen corruption families follows exactly from the algebraic changes in $V - E + F$; it is therefore a verification of the software and diagnostic interpretation rather than an empirical law about all mesh corruption. More subtle errors can preserve Euler characteristic. An edge flip, vertex relocation, or even paired topological changes with cancelling Euler contributions can leave $R_\chi = 0$. Non-manifold structures can also require additional diagnostics even though Equation (11) still performs correct incidence accounting.

A robust production validator should therefore combine R_χ with explicit manifold checks: every triangle should contain three distinct valid vertex indices; duplicate faces should be disallowed unless the data model explicitly permits them; each interior edge of a two-manifold terrain should be incident to two faces and each boundary edge to one; and vertex links should have the expected cycle or path structure. The present method is best viewed as a global checksum with a mathematically interpretable local decomposition, not a replacement for structural validation.

5.5. Earth-Science Relevance and Journal Positioning

TINs are already operational objects in hydrological and land-surface modeling [1] and in coastal ocean mesh generation [2]. A topology audit is therefore relevant at data-ingestion, remeshing, model-coupling and export stages. In workflows that create a terrain mesh from raster or point-cloud data, the audit can be stored alongside standard mesh-quality metadata. During processing, changes in the expected Euler characteristic can then be attributed to intentional domain edits or flagged for inspection.

The filtration component is relevant when the mesh is not only a computational support but also an analysis representation. TDA has already shown usefulness for Earth-observation morphology, including landslide analysis [10]. Our results emphasize that representation choices must be included in the uncertainty budget for such methods. The proposed ensemble protocol offers one inexpensive way to do so before moving to more detailed persistent-homology analyses.

5.6. Limitations

Several limitations bound the claims of this study. First, both surfaces are public benchmark arrays bundled with a plotting library rather than newly acquired field or national-mapping-agency products. Their role is reproducible method validation. A follow-up domain study should repeat the protocol on authoritative DEM/LiDAR products with documented horizontal and vertical datums and terrain-specific ground truth.

Second, the four triangulation rules are deliberately simple. Constrained Delaunay, feature-preserving, hydrologically conditioned, adaptive-error and model-specific meshes may produce different uncertainty envelopes. Third, the geometric metric uses plan-view triangles only. Numerical PDE meshes may require three-dimensional quality measures, conditioning metrics or solver-specific criteria. Fourth, the static Euler residual detects only discrepancies that alter the expected Euler characteristic; it cannot certify manifoldness or geometric validity. Fifth, an ECC is a compressed topological summary and does not retain the full information of persistent homology.

Finally, this paper validates a computational Earth-science method rather than making a new geological interpretation of the Jacksboro fault or Pacific Northwest morphology. That separation is intentional: the method should first be audited on transparent inputs before being used to support process-level claims.

6. Conclusions

We developed and implemented a topology-aware quality-control framework for triangulated terrain models. A boundary-aware affine classification shows that a local degree/face-count functional has a refinement-invariant total precisely when $A + 6B + 2C = 0$ and $T = 2B + C$. The canonical normalization given in Equation (10) provides an exact local decomposition of Euler characteristic for any finite triangular complex.

On two real Earth-surface benchmark arrays, 32 valid meshes spanning four triangulation rules and four resolutions satisfied the static identity to floating-point precision. Controlled topological defects changed the residual exactly as predicted, while topology-preserving diagonal changes did not. A coordinate sliver demonstrated the complementary failure mode of geometry: it left the topology audit unchanged while collapsing minimum angle and element quality. Elevation-filtration ECCs then exposed information that the static invariant cannot: intermediate topology varied measurably across valid triangulations and resolutions, and raster 4/8-connectivity differences were even larger in the tested examples.

The main practical recommendation is therefore not a single new curvature map, but an auditable workflow: first, verify expected global topology with local Euler accounting; second, verify triangle geometry independently; and third, report representation sensitivity for topology-derived terrain descriptors. The supplied implementation is compact enough to be inserted into existing geospatial preprocessing pipelines and provides a reproducible basis for testing on authoritative DEM, LiDAR, hydrological and coastal modeling data sets.

Data and Code Availability

The exact input arrays used for the numerical benchmarks, all Python scripts, generated CSV/JSON result tables and vector figures are supplied in the accompanying supplementary package. The two input arrays are public Matplotlib sample data; the analysis scripts operate directly on the included copies so that every reported numerical result can be reproduced without network access.

Author Contributions

Conceptualization, methodology, software, validation, formal analysis, investigation, data curation, writing of the original draft, review and editing, and visualization were all carried out by Bekarys Tashmukhanbet. The author has read and agreed to the published version of the manuscript.

Conflicts of Interest

The author declares no conflicts of interest regarding the publication of this paper.

References

[1] Marsh, C.B., Spiteri, R.J., Pomeroy, J.W. and Wheater, H.S. (2018) Multi-Objective Unstructured Triangular Mesh Generation for Use in Hydrological and Land Surface Models. *Computers & Geosciences*, **119**, 49-67. https://doi.org/10.1016/j.cageo.2018.06.009

[2] Roberts, K.J., Pringle, W.J. and Westerink, J.J. (2019) OceanMesh2D 1.0: MATLAB-Based Software for Two-Dimensional Unstructured Mesh Generation in Coastal Ocean Modeling. *Geoscientific Model Development*, **12**, 1847-1868. https://doi.org/10.5194/gmd-12-1847-2019

[3] do Carmo, M.P. (1976) Differential Geometry of Curves and Surfaces. Prentice-Hall, Englewood Cliffs.

[4] Bobenko, A.I. and Suris, Y.B. (2008) Discrete Differential Geometry: Integrable Structure. American Mathematical Society, Providence. https://doi.org/10.1090/gsm/098

[5] Higuchi, Y. (2001) Combinatorial Curvature for Planar Graphs. *Journal of Graph Theory*, **38**, 220-229. https://doi.org/10.1002/jgt.10004

[6] Knill, O. (2011) A Graph Theoretical Gauss-Bonnet-Chern Theorem. arXiv: 1111.5395. https://arxiv.org/abs/1111.5395

[7] Meyer, M., Desbrun, M., Schröder, P. and Barr, A.H. (2003) Discrete Differential-Geometry Operators for Triangulated 2-Manifolds. In: Hege, H.-C. and Polthier, K., Eds., *Visualization and Mathematics III*, Springer, Berlin, 35-57. https://doi.org/10.1007/978-3-662-05105-4_2

[8] Hu, G., Xiong, L., Lu, S., Chen, J., Li, S., Tang, G. and Strobl, J. (2022) Mathematical Vector Framework for Gravity-Specific Land Surface Curvatures Calculation from Triangulated Irregular Networks. *GIScience & Remote Sensing*, **59**, 590-608. https://doi.org/10.1080/15481603.2022.2044149

[9] Stupariu, M.-S. (2021) Discrete Curvatures of Triangle Meshes: From Approximation of Smooth Surfaces to Digital Terrain Data. *Computers & Geosciences*, **153**, Article ID: 104789. https://doi.org/10.1016/j.cageo.2021.104789

[10] Syzdykbayev, M., Karimi, B. and Karimi, H.A. (2020) Persistent Homology on LiDAR Data to Detect Landslides. *Remote Sensing of Environment*, **246**, Article ID: 111816. https://doi.org/10.1016/j.rse.2020.111816

[11] Dłotko, P. and Gurnari, D. (2023) Euler Characteristic Curves and Profiles: A Stable Shape Invariant for Big Data Problems. *GigaScience*, **12**, giad094. https://doi.org/10.1093/gigascience/giad094

[12] Hunter, J.D. (2007) Matplotlib: A 2D Graphics Environment. *Computing in Science & Engineering*, **9**, 90-95. https://doi.org/10.1109/MCSE.2007.55

[13] Englund, K.J. (1968) Geology and Coal Resources of the Elk Valley Area, Tennessee and Kentucky. U.S. Geological Survey Professional Paper 572, U.S. Geological Survey, Washington DC. https://doi.org/10.3133/pp572

[14] Edelsbrunner, H. and Harer, J. (2010) Computational Topology: An Introduction. American Mathematical Society,

Providence. https://doi.org/10.1090/mbk/069

[15] van der Walt, S., Schönberger, J.L., Nunez-Iglesias, J., Boulogne, F., Warner, J.D., Yager, N., Gouillart, E. and Yu, T. (2014) Scikit-Image: Image Processing in Python. *PeerJ*, **2**, e453. https://doi.org/10.7717/peerj.453

[16] Harris, C.R., Millman, K.J., van der Walt, S.J., Gommers, R., Virtanen, P., Cournapeau, D., et al. (2020) Array Programming with NumPy. *Nature*, **585**, 357-362. https://doi.org/10.1038/s41586-020-2649-2